J. Fluid Mech. (2002), *vol.* 466, *pp.* 85–111.
DOI: 10.1017/S0022112002001106 Printed in the United Kingdom

Surfactant transport on highly viscous surface films

By O. K. MATAR[1], R. V. CRASTER[2] AND M. R. E. WARNER[2]

[1]Department of Chemical Engineering and Chemical Technology, Imperial College of Science, Technology and Medicine, London SW7 2BY, UK
[2]Department of Mathematics, Imperial College of Science, Technology and Medicine, London SW7 2BZ, UK

(Received 9 April 2001 and in revised form 4 March 2002)

We examine surfactant transport on a highly viscous film overlying a much less viscous layer, aimed at situations within the smaller pulmonary airways, wherein the highly viscous film corresponds to the mucus layer, that rides atop the Periciliary liquid layer (PCL). To this end, we generate a variant of the lubrication approximation by promoting terms which would have otherwise been neglected within standard lubrication theory; this is reminiscent of theories involving free films, viscous jets and threads. We also account for the presence of van der Waals forces, which could rupture the thin bilayer fluid coating the small airways. This is a potential difficulty for surfactant replacement therapy (SRT) since rupture will leave behind pools of stranded surfactant thereby restricting the levels reaching the smallest airways and potentially leading to clinical failure. In the present study, the presence of the mucus layer and its effect on the spreading characteristics and film rupture is investigated for a wide range of system parameters using analytical techniques and numerical simulations.

1. Introduction

Surfactant replacement therapy for the treatment of respiratory distress syndrome (RDS) both in neonates and adults (Robertson 1984) is widely used and relies upon external delivery of surfactant into the diseased lungs. RDS is manifested by airway closure, oedema, and decreased lung compliance, often with fatal consequences. Surfactant is also utilized to transport chemicals for various treatments to lung diseases, and is proposed as a delivery mechanism for gene therapies (Banerjee & Puniyani 2000). Achieving a fundamental understanding of the surfactant delivery process has led to considerable interest in modelling surfactant spreading on the surface of thin liquid films (Borgas & Grotberg 1988; Gaver III & Grotberg 1990; Jensen & Grotberg 1992; Espinosa *et al.* 1993; Grotberg 1994; Grotberg, Halpern & Jensen 1995; Halpern, Jensen & Grotberg 1998; Espinosa & Kamm 1999) which represent the liquid lining of pulmonary airways. Until recently, these modelling studies had focused on the dynamics of a single Newtonian layer, taking into account Marangoni stresses, surface diffusion, gravity, capillarity and intermolecular forces, in both simple and complex lung geometries. The thin liquid lining of pulmonary airways, however, is in fact a bilayer consisting of a non-Newtonian mucus layer overlying a Newtonian watery Periciliary liquid layer (PCL). The bilayer situation is also of interest in coating flows, and highly viscous surface layers are important in foams where Marangoni forces can also be present (Naire, Braun & Snow 2000).

Recently, Craster & Matar (2000, hereafter referred to as Paper I), have extended the modelling to incorporate this bilayer nature of the airway lining, and the shear thinning and yield stress components of mucus rheology. Their results demonstrate that the flow profiles and surfactant spreading rates can be greatly affected by mucus rheology. In particular, they showed that the time taken to recover Newtonian spreading rates increases with increasing mucus yield stress and shear-thinning character. In these cases, they also showed that spreading was accompanied by the formation of large mucus peaks concentrated at the surfactant leading edge; these peaks could potentially cause airway blockage, another undesirable clinical feature. The majority of these results, however, were obtained with a mucus to PCL thickness ratio of 3 : 1, which may be more reflective of the clinical conditions in the upper airways wherein surfactant transport may be influenced, or indeed primarily driven, by gravity. Nevertheless, the results should still be applicable to medical conditions, such as cystic fibrosis, which can significantly affect the depth of the mucus layer throughout the lung, and to some models of bolus insertion in the upper airways, which assume Marangoni-driven flows (Halpern *et al.* 1998). However, dependent upon the respiratory ailment, this ratio is likely to vary across the generations in the pulmonary tree and may be much smaller in the lower airways (Sleigh 1991).

We focus on modelling the spreading characteristics in the smaller airways wherein spreading on the thin mucus films is wholly Marangoni driven. The rheology of mucus can also vary substantially between individuals, clinical conditions, and even lung generation, with mucus viscosities for some diseases apparently several orders of magnitude greater than those of the watery PCL; thus, surfactant spreads on the surface of a highly viscous mucus film overlying a PCL layer. This spreading process is modelled here by generating a highly viscous 'skin' theory somewhat reminiscent of the Boussinesq–Scriven surface viscosity theory (Scriven 1960) or the embedded highly viscous strands used to model highly elongated polymers in high Deborah number flows (Harlen, Rallison & Chilcott 1990) but derived here using lubrication scalings. The approach taken here is very similar to that often used to generate the equations governing the evolution of free films (Erneux & Davis 1993; De Wit, Gallez & Christov 1994) and of thin viscous threads and jets (Papageorgiou 1995*a*, *b*; Ida & Miksis 1998*a*, *b*; Craster, Matar & Papageorgiou 2002) using the long wavelength approximation. Numerical simulations together with similarity scalings are utilized to investigate whether this induces any changes in the transport rates predicted by the single-layer (Jensen & Grotberg 1992) and bilayer (Paper I) theories. The effect of the presence of the skin on the possibility of film rupture, a potential difficulty in surfactant replacement therapy, is also investigated; non-uniform spreading and insufficient amounts of surfactant reaching the smaller airways potentially lead to clinical failure. Although the rupture of thin pure liquid films, or a uniformly surfactant coated film, has been a well-studied problem (Ruckenstein & Jain 1974; Williams & Davis 1982; Sharma & Ruckenstein 1986; Zhang & Lister 1999; Witelski & Bernoff 1999, 2000) potential rupture instabilities associated with a spreading monolayer have been less well studied (Jensen & Grotberg 1992). We shall focus on the highly viscous nature of the bilayer and isolate these effects from non-Newtonian effects even though mucus is known to possesses considerable non-Newtonian rheological characteristics.

The rest of the paper is organized as follows: the problem is formulated in § 2. In § 3, we present similarity solutions of the evolution equations describing the spreading process and full numerical solutions are provided in § 4. Finally, concluding remarks are provided in § 5.

2. Formulation

Our aim is to take advantage of the remarkably thin fluid layers that exist in the lung, and high mucus viscosities, to determine a reduced set of evolution equations that capture the essential dynamics.

2.1. *The governing equations*

Two thin films of Newtonian, incompressible, immiscible, fluids are bounded from below by a horizontal, rigid and impermeable solid substrate located at $z = 0$. The upper layer consists of mucus of viscosity η and density ρ, while the lower layer is the Periciliary liquid layer (PCL) of viscosity $\bar{\eta}$ and density $\bar{\rho}$; all material variables associated with the PCL have the distinguishing overbar. A dilute monolayer of insoluble surfactant is introduced at the air–mucus interface, which is located at $z = h(x,t)$; the surface tension of this interface is denoted by $\sigma(x,t)$. This surfactant, whose concentration is denoted by $\Gamma(x,t)$, will be referred to as exogenous; any surfactant already present on $z = h(x,t)$ is endogenous. The influence of endogenous surfactant on the spreading dynamics has been well studied (Espinosa *et al.* 1993; Grotberg *et al.* 1995; Bull *et al.* 1999) and will not be considered in the present work.

Surfactant solubility is an issue that could be important in applications, and has been considered by Halpern & Grotberg (1992) and Jensen & Grotberg (1993); this involves incorporating an advection–diffusion equation for surfactant concentration within the liquid layer into the analysis. We shall leave this issue aside and concentrate upon developing the present highly viscous theory for insoluble surfactant. From the insoluble assumption it follows that the mucus–PCL interface, $z = \bar{h}(x,t)$, is devoid of surfactant, hence its surface tension will remain a constant denoted by $\bar{\sigma}$. The action of the cilia, which are potentially present within the PCL, will also be ignored in the present work. Variations in surfactant concentration along the upper surface $z = h(x,t)$ give rise to gradients in the surface tension, $\sigma(x,t)$, that, in turn, induce surface stresses that drive surfactant transport in the direction of the uncontaminated air–mucus interface. This Marangoni-driven fluid motion is described by the velocity field, $\boldsymbol{u} = (u(x,z,t), w(x,z,t))$ with origin at the centre of the surfactant deposition, while pressure is denoted by $p(x,z,t)$.

Conservation of momentum and mass in the mucus layer yield

$$\rho\frac{\mathrm{D}\boldsymbol{u}}{\mathrm{D}t} = -\nabla(p+\phi) + \rho\boldsymbol{g} + \nabla\cdot\boldsymbol{\tau}, \quad \nabla\cdot\boldsymbol{u} = 0, \tag{2.1}$$

where τ_{ij} denotes the components of the deviatoric stress tensor and $\boldsymbol{g}$ is acceleration due to gravity. The equations for the lower layer are identical save for the addition of an overbar. The stresses are related to the strain rates via $\tau_{ij} = \eta\dot{\gamma}_{ij}$, where the viscosity $\eta = \eta_0\hat{\eta}$ with η_0 as a reference viscosity. The usual conservation-of-momentum equations are augmented by ϕ, a potential energy per unit volume in the liquid bilayer representing the presence of van der Waals forces. The potential within the mucus layer, ϕ, represents an interaction between the air–mucus interface and the base, and an interaction between the mucus–PCL interface and the air–mucus interface. The potential within the PCL layer, $\bar{\phi}$, represents an interaction between the air–mucus interface and the base, and an interaction between the mucus–PCL interface and the base. These potentials are given by Israelachvili (1985):

$$\phi(x,t) = \frac{\mathscr{A}_1}{h^3} + \frac{\mathscr{A}_2}{(h-\bar{h})^3} \quad \text{for} \quad \bar{h} < z < h, \quad \bar{\phi}(x,t) = \frac{\mathscr{A}_3}{h^3} + \frac{\mathscr{A}_4}{\bar{h}^3} \quad \text{for} \quad 0 < z < \bar{h}, \tag{2.2}$$

where the $\mathscr{A}_i$ are four different so-called Hamaker constants; for a single layer only a single Hamaker constant appears. The gradient of this potential represents the force per unit volume due to intermolecular forces; other intermolecular forces such as, for instance, electric double layer forces, will not be considered here.

Although the complex rheological properties of mucus, such as yield stress and shear thinning (Paper I) as well as viscoelasticity, play a significant role in the dynamics of the spreading process, in this paper we shall concentrate on the situation in which mucus is treated as a Newtonian fluid, but having a much higher viscosity than that of the underlying PCL layer. This assumption is supported by order-of-magnitude estimates of the viscosity found in the biomedical literature (Silberberg 1983). Different clinical conditions lead to widely varying values for mucus viscosity; in some circumstances the viscosity mismatch may be less dramatic and our earlier theory, Paper I, is appropriate.

The concentration of surfactant at the surface, $\Gamma(x,t)$, satisfies a surface transport equation (Stone 1990),

$$\Gamma_t + \nabla_s \cdot (\boldsymbol{u}_s \Gamma) + (\nabla_s \cdot \boldsymbol{n})\Gamma(\boldsymbol{u}\cdot\boldsymbol{n}) = \mathscr{D}\nabla_s^2\Gamma \tag{2.3}$$

on $z = h(x,t)$; the surface gradient operator, ∇_s, is defined $\nabla_s = [\boldsymbol{I} - \boldsymbol{n}\,\boldsymbol{n}]\cdot\nabla \equiv \boldsymbol{I}_s\cdot\nabla$ and $\boldsymbol{u}_s$ is the surface velocity: $\boldsymbol{u}_s = \boldsymbol{I}_s\cdot\boldsymbol{u}$; and $\mathscr{D}$ denotes the surface diffusion coefficient. The normal to the free surface, $\boldsymbol{n}$, is defined $\boldsymbol{n} = (-h_x, 1)/\sqrt{h_x^2+1}$.

These equations are solved subject to appropriate boundary conditions. No slip is imposed at the solid substrate,

$$u = 0 \quad \text{and} \quad w = 0 \quad \text{on} \quad z = 0. \tag{2.4}$$

At the mucus–air interface, $z = h(x,t)$, we have the kinematic boundary condition

$$h_t + uh_x = w, \tag{2.5}$$

together with stress boundary conditions expressed by

$$(\boldsymbol{\tau} - \boldsymbol{I}p)\cdot\boldsymbol{n} = \sigma\kappa\boldsymbol{n} + \nabla_s\sigma, \tag{2.6}$$

in which $\kappa = \nabla_s\cdot\boldsymbol{n}$ denotes the curvature of the air-mucus interface. At the mucus-PCL interface, $z = \bar{h}(x,t)$, the velocities are continuous and the kinematic condition is $\bar{h}_t + \bar{u}\bar{h}_x = \bar{w}$. We also assume that the stresses are continuous at $z = \bar{h}$, and since the surfactant is insoluble $\nabla_s\bar{\sigma} = 0$.

As it stands the system of governing equations and their related boundary conditions form a complicated coupled system. Asymptotic reduction to a simpler, but still physically relevant, system follows by utilizing the small aspect ratio arising from the remarkably thin fluid films that line the airways. Separate scalings will be chosen for two situations, negligible and significant van der Waals forces, leading to the derivation of two separate sets of dimensionless coupled evolution equations.

2.2. *Negligible van der Waals forces*

2.2.1. *Scaling*

The governing equations in the absence of van der Waals forces are rendered dimensionless using scalings that balance viscous stresses with the driving Marangoni forces. Using the familiar route of a lubrication-style analysis we utilize a characteristic thickness of the fluid layer, $\mathscr{H}$, as the dimension of z, and $\mathscr{L}$ as the characteristic horizontal length scale; ultimately we set $\epsilon = \mathscr{H}/\mathscr{L} \ll 1$. We measure the speed u by

$\mathscr{V}$, w by $\mathscr{H}\mathscr{V}/\mathscr{L}$, and time by $\mathscr{L}/\mathscr{V}$ so that

$$x = \mathscr{L}\tilde{x}, \quad z = \mathscr{H}\tilde{z}, \quad u = \mathscr{V}\tilde{u}, \quad w = (\mathscr{V}\mathscr{H}/\mathscr{L})\tilde{w}, \quad t = (\mathscr{L}/\mathscr{V})\tilde{t}, \quad h = \mathscr{H}\tilde{h}, \quad (2.7)$$

in which the tilde denotes dimensionless quantities. To non-dimensionalize the equations involving the surfactant and surface tension we introduce

$$\sigma = \sigma_m + \mathscr{S}\,\tilde{\sigma}, \quad \Gamma = \Gamma_m\tilde{\Gamma}. \quad (2.8)$$

The terms Γ_m and σ_m represent concentration of surfactant and surface tension, respectively, of the most contaminated part of the interface; $\mathscr{S} = \sigma_0 - \sigma_m$ corresponds to the spreading pressure wherein σ_0 is the surface tension of a perfectly clean, surfactant-free interface. For pressure we introduce $p = \mathscr{S}\tilde{p}/\mathscr{H}$. We then select the following characteristic velocity and pressure scales by balancing Marangoni stresses with viscous retardation:

$$\mathscr{V} = \frac{\mathscr{S}\mathscr{H}}{\eta_0\mathscr{L}}, \quad \mathscr{P} = \frac{\mathscr{S}}{\mathscr{H}}, \quad (2.9)$$

where $\mathscr{P}$ is the pressure scale. The strain rates and stresses then scale as follows:

$$\tau_{ij} = \frac{\mathscr{S}}{\mathscr{L}}\tilde{\tau_{ij}}, \quad \dot{\gamma}_{ij} = \frac{\mathscr{S}}{\eta_0\mathscr{L}}\tilde{\dot{\gamma}_{ij}}. \quad (2.10)$$

From here on we shall consider non-dimensionalized variables and we drop the tilde. It emerges that the Reynolds number, $Re \equiv \rho\mathscr{H}\mathscr{V}^2/\mathscr{S}$, and Bond number, $\mathscr{G} \equiv \rho g\mathscr{H}^2/\mathscr{S}$, which gives a measure of the relative importance of gravity and surface tension gradients, are both very small for typical values that are relevant to the application (table 2 of Paper I) and are henceforth neglected. Finally, we ignore capillary effects in the analysis of surfactant spreading in the absence of van der Waals forces. These capillary terms, however, will be reintroduced later when we investigate van-der-Waals-driven bilayer rupture.

The rates of strain, $\dot{\gamma}_{ij}$, are given by

$$\dot{\gamma}_{ij} = \begin{pmatrix} 2\epsilon u_x & u_z + \epsilon^2 w_x \\ u_z + \epsilon^2 w_x & 2\epsilon w_z \end{pmatrix} \quad (2.11)$$

and are related to the stresses, τ_{ij}, via

$$\tau_{ij} = \hat{\eta}(z)\dot{\gamma}_{ij}, \quad \hat{\eta}(z) = \begin{cases} \eta_1/\epsilon^2, & d < z < h \\ 1, & 0 < z < d. \end{cases} \quad (2.12)$$

Thus, in the mucus layer we have set the viscosity to $\hat{\eta} = \eta_1/\epsilon^2$, that is, we force the viscosity to be very large and this promotes several terms, which, in lubrication theory, would have normally been ignored. In the PCL layer, on the other hand, $\hat{\eta} = 1$ and we obtain familiar equations, although since the motion is coupled to the upper layer it still 'feels' the influence of the highly viscous mucus layer. This assumption regarding the viscosity of the mucus, that it is much larger than that of the PCL layer, is vital in our development of the theory. In terms of the asymptotic expansion pursued later, this enables us to select the appropriate terms in the modified lubrication approximation that account for the enhanced resistance to flow.

Similar large viscosity contrasts between a surface layer and an underlying film occur in several other contexts, for instance in cooling lava flows (Balmforth & Craster 2002) where the fluid has either a highly temperature-dependent viscosity or is developing a solid surface crust, or both. Although the viscosity and fluid motion

coupling with an evolving thermal boundary layer complicates matters, related ideas can be pursued (Balmforth & Craster 2002). Similar ideas also arise in ice flows where the ice and melt water have dramatically different viscosities (Toniolo 2001).

2.2.2. *The dimensionless thin layer equations*

Substitution of the scalings defined above into the governing equations, constitutive relations and boundary conditions and formally letting $\epsilon \to 0$ leads to the reduced form of the governing equations, in the so-called lubrication limit. Note, however, that due to the earlier viscosity assumption we shall retain more terms than is normally the case. We list the dimensionless thin-layer equations in the mucus and PCL layers, as well as the associated boundary conditions at the interfaces $z = h$ and $z = \bar{h}$, and base, $z = 0$.

In the mucus layer, the equations of momentum conservation and the continuity equation become

$$\epsilon^2 p_x = \eta_1(u_{zz} + \epsilon^2 u_{xx}), \quad p_z = \eta_1(w_{zz} + \epsilon^2 w_{xx}), \quad u_x + w_z = 0, \tag{2.13}$$

plus higher-order terms. In the underlying PCL layer, the equations are

$$\bar{p}_x = \bar{u}_{zz} + \epsilon^2 \bar{u}_{xx}, \quad \bar{p}_z = \epsilon^2(\bar{w}_{zz} + \epsilon^2 \bar{w}_{xx}), \quad \bar{u}_x + \bar{w}_z = 0. \tag{2.14}$$

At $z = h(x,t)$ the normal and shear stress boundary conditions are expressed by

$$p = \eta_1 h_x u_z - 2\eta_1 u_x + O(\epsilon^2), \quad \eta_1 \left(\frac{u_z}{\epsilon^2} + w_x - 2h_x u_x \right) + h_x p = \sigma_x + O(\epsilon^2), \tag{2.15}$$

while the kinematic boundary condition and the surfactant transport equation are given by

$$h_t + \frac{\partial}{\partial x} \int_0^h u \, \mathrm{d}z = 0, \quad \Gamma_t + (u_s \Gamma)_x = \frac{1}{Pe} \Gamma_{xx}, \tag{2.16}$$

where Pe is the Péclet number.

At the interface, $z = \bar{h}(x,t)$, we have continuity of velocity, $u = \bar{u}$ and $w = \bar{w}$, in addition to continuity of the normal and shear stresses, respectively expressed by

$$p - \bar{p} = \eta_1(2w_z - \bar{h}_x u_z), \quad \bar{u}_z = \eta_1 \left(\frac{u_z}{\epsilon^2} + w_x - 2\bar{h}_x u_x \right) + \bar{h}_x (p - \bar{p}). \tag{2.17}$$

Additionally, we have the kinematic boundary condition:

$$\bar{h}_t + \frac{\partial}{\partial x} \int_0^{\bar{h}} \bar{u} \, \mathrm{d}z = 0. \tag{2.18}$$

At $z = 0$, the no-slip and no-penetration conditions are imposed: $\bar{u} = 0$, $\bar{w} = 0$.

We expand all variables in powers of ϵ as $u = u_0 + \epsilon^2 u_2 + \cdots$, $w = w_0 + \epsilon^2 w_2 + \cdots$, with a similar expansion for the other variables and analogous quantities in the PCL layer; these are substituted into the governing equations and boundary conditions and terms of the same order are collected. Our ultimate aim is the derivation of evolution equations that govern the total height, mucus layer depth and surfactant distribution, and it will turn out that we require an evolution equation for the mucus velocity. Hence, there are close connections with similar equations derived for free films, viscous threads and jets in the presence and absence of surfactant (Erneux & Davis 1993; De Wit *et al.* 1994; Papageorgiou 1995*a*, *b*; Ida & Miksis 1998*a*, *b*; Craster *et al.* 2001) where the dynamics of the exterior fluid (air in all cases) have been neglected. Details of the derivation of the evolution equations for the mucus

velocity, air–mucus interface, mucus–PCL interface and surfactant concentration are provided in the Appendix.

2.2.3. *The evolution equations*

The full system of coupled evolution equations is

$$h_{0t} = -\left[u_0\left(h_0 - \frac{\bar{h}_0}{2}\right)\right]_x, \quad \Gamma_{0t} = -[u_0\Gamma_0]_x + \frac{1}{Pe}\Gamma_{0xx}, \tag{2.19}$$

$$\bar{h}_{0_t} = -\left[\frac{u_0\bar{h}_0}{2}\right]_x, \quad u_0 = \bar{h}_0(\sigma_{0x} + 4\eta_1[d_0 u_{0x}]_x), \tag{2.20}$$

in which d_0 is the thickness of the mucus layer. This coupled system of evolution equations governs the surfactant-driven flow for a thin fluid bilayer where the upper layer is highly viscous. As noted by Erneux & Davis (1993) the $4\eta_1\delta_0$ is not coincidental: it has an interpretation as the Trouton viscosity, that is, the ratio of extensional to shear viscosities in simple Newtonian flow. Note that in the limit $\eta_1 \to 0$ and $h_0 = \bar{h}_0$, the above equations reduce to those describing the spreading of an insoluble surfactant monolayer on a single, thin Newtonian layer (Jensen & Grotberg 1992).

A surfactant equation of state is needed to close the above system of equations. Since the primary objective of the present work is to investigate the effect of large viscosity contrast between the mucus and PCL layers, we restrict ourselves to a simple linear equation of state, $\sigma = 1 - \Gamma$, although nonlinear laws are often used in practice (Gaver III & Grotberg 1990; Jensen & Grotberg 1992).

At this point, it is, perhaps, worth comparing the current theory with the classical 'skin' viscosity theory of Boussinesq and Scriven (Scriven 1960; Edwards, Brenner & Wasan 1991), which considers a surface skin of infinitesimal thickness having a surface viscosity. This introduces a restraining force at the surface which is the product of a so-called dilatational viscosity multiplied by the rate of expansion of the surface; we shall ignore shear surface viscosity effects. That theory is derived in a different manner, not based upon highly viscous skins with a variable skin depth, but from the consideration of mass and momentum balances upon a deforming infinitesimally thin interface. If one proceeds using that theory, arbitrarily increasing the dilatational viscosity, λ, by an order $1/\epsilon^2$ to mimic the highly viscous mucus, one obtains the following evolution equations:

$$h_{0t} + \left[\frac{h_0}{2}u_0\right]_x = 0, \quad \Gamma_{0t} + [u_0\Gamma_0]_x = \frac{1}{Pe}\Gamma_{0xx}, \quad u_0 = h_0[\lambda u_{0xx} + \sigma_{0x}] \tag{2.21}$$

(see also Jensen & Grotberg 1992). Once again the crucial equation is that for an evolving surface velocity, $u_0(x, t)$. We recover (2.21) from equations (2.19)–(2.20) by taking the simultaneous limit that $\eta_1 \to \infty$ whilst $\delta_0 \to 0$ such that $\eta_1\delta_0 \to \lambda$ and $\eta_1\delta_{0x} \to 0$; there are minor differences in the final equations in the axisymmetric case if this is done. Nonetheless, it is clear that both approaches are closely related and one could use the arguments presented here as a justification for the use, and interpretation, of surface viscosity; several recent papers utilize the surface viscosity theory directly, for instance Naire *et al.* (2000) analyse drainage of thin films covered with insoluble surfactant in the limit of high surface viscosity.

2.3. *Significant van der Waals forces*

In the absence of surfactant, van-der-Waals-driven thin-film rupture has recently been of renewed and considerable interest. For a single layer, in the absence of surfactant-

driven flows, Zhang & Lister (1999*a*, *b*) and Witelski & Bernoff (1999, 2000) have shown that forces due to surface tension, van der Waals and viscous dissipation are all important near the rupture event; this is in contrast to other earlier analyses (Burelbach, Bankoff & Davis 1988) that assumed surface tension was asymptotically negligible there. These recent papers give scalings for the rate of thinning of the thin liquid layer and detail similarity solutions; our aim is complementary, but we now include surfactant and a thin highly viscous 'skin'. This proposed system has previously been studied in the simplified Newtonian single-layer limit by Jensen & Grotberg (1992). We now aim to formulate the governing equations for a thin, highly viscous mucus layer overlying a much less viscous PCL layer, taking into account both capillary and van der Waals forces.

2.3.1. *Scaling*

The chosen scalings remain largely unchanged from § 2.2.1 with the exception of the pressure and velocity scalings. We select

$$\mathscr{V} = \mathscr{A}/\eta_0 \mathscr{H}\mathscr{L}, \quad \mathscr{P} = \mathscr{A}/\mathscr{H}^3, \tag{2.22}$$

in order to balance pressure with van der Waals forces and viscous retardation with the pressure and van der Waals terms; these are the dominant physical processes in the rupture regime. Here, $\mathscr{A}$ is a typical Hamaker constant value (so that $\mathscr{A}_i = \mathscr{A}A_i$, $i = 1, 2, 3, 4$, the A_i-being the nondimensional Hamaker constants). Substitution of these scalings into the governing equations and boundary conditions and neglecting inertial and gravitational terms yields a similar set of dimensionless thin-layer equations to those encountered in § 2.2.2, except for the appearance of the van der Waals and capillary terms. A dimensionless Marangoni parameter, $\mathscr{M}$, also emerges which reflects the significance of Marangoni stresses to van der Waals forces:

$$\mathscr{M} = \frac{\mathscr{H}\mathscr{S}}{\eta_o \mathscr{L}\mathscr{V}} \equiv \frac{\mathscr{H}^2\mathscr{S}}{\mathscr{A}}. \tag{2.23}$$

If we consider typical values (de Souza & Gallez 1998) of $\mathscr{A} \sim 10^{-13}$ erg and $\sigma_m \sim 10\,\mathrm{dyn\,cm^{-1}}$, then choosing different values for the characteristic fluid thickness we can estimate the Marangoni number. First, if $\mathscr{H} \sim 10^{-5}$ cm, we have $\epsilon = 10^{-2}$ and $\mathscr{M} = 10^3 S$. In this circumstance surface tension gradients potentially dominate van der Waals and capillarity effects, and we recover our earlier analysis. To investigate Marangoni effects on rupture we take $S = \epsilon^2 s$, that is, a weak spreading pressure more representative of the actual conditions at the inception of rupture. The net effect of choosing this scaling is that the pressure in the layer is now

$$p_0 = -\left(1 + \frac{\epsilon^2 s \sigma_0}{\sigma_m}\right)\kappa,$$

and the contribution to the spreading process from capillarity, which is now constant, and that due to surface tension gradients, the order-ϵ^2 term, separate (Jensen & Grotberg 1992). For much thinner fluid layers, say $\mathscr{H} \sim 10^{-7}$ cm with $\mathscr{A} \sim 10^{-14}$ erg and $\sigma_m \sim 10\,\mathrm{dyn\,cm^{-1}}$ then $\epsilon \sim 10^{-1/2}$ and $\mathscr{M} \sim S$. In this case it may be possible that surface tension gradients could also affect capillarity. We have explored this possibility and found the results to be largely unchanged. In the interests of brevity, therefore, we do not consider this possibility further in the present work and in the remainder of the text we take $\mathscr{S} = \epsilon^2 s$; thus, terms involving $\mathscr{S}$ make negligible contribution and are henceforth ignored.

2.3.2. *The evolution equations*

Following the same procedure as in § 2.2.2 and the Appendix, we obtain the following equation for the velocity in the mucus layer:

$$u_0(x,t) = -\frac{\bar{h}_0^2}{2}(\bar{p}_0 + \bar{\phi}_0)_x - \bar{h}_0 d_0 (p_s + \phi_0)_x + (4\eta_1 [d_0 u_{0_x}]_x + \mathscr{M}\sigma_{0x})\bar{h}_0, \tag{2.24}$$

where p_s, the pressure due to the air–mucus curvature, and $\bar{p}_0$, are expressed by

$$p_s = -\kappa = -h_{0xx}, \quad \bar{p}_0 = -\kappa - \bar{\kappa} = -(h_{0xx} + \bar{h}_{0xx}). \tag{2.25}$$

The evolution equations for h_0, $\bar{h}_0$ and Γ_0 are

$$h_{0t} = -\left[u_0\left(h_0 - \frac{\bar{h}_0}{2}\right)\right]_x + \frac{1}{12}[\bar{h}_0^3(\bar{p}_0 + \bar{\phi}_0)_x]_x, \tag{2.26}$$

$$\bar{h}_{0t} = -\left[\frac{u_0\bar{h}_0}{2}\right]_x + \frac{1}{12}[\bar{h}_0^3(\bar{p}_0 + \bar{\phi}_0)_x]_x, \quad \Gamma_{0t} = -[u_0\Gamma_0]_x + \frac{1}{Pe}\Gamma_{0xx}. \tag{2.27}$$

The potentials, $\phi_0(x,t)$ and $\bar{\phi}_0(x,t)$, follow from an expansion of equation (2.2):

$$\phi_0(x,t) = \frac{A_1}{h_0^3} + \frac{A_2}{d_0^3} \quad \text{for} \quad \bar{h}_0 < z < h_0, \quad \bar{\phi}_0(x,t) = \frac{A_3}{h_0^3} + \frac{A_4}{\bar{h}_0^3} \quad \text{for} \quad 0 < z < \bar{h}_0. \tag{2.28}$$

Setting the A_i to zero, $\mathscr{M} = 1$ and omitting the capillary terms, equations (2.24)–(2.27) become identical to equations (2.19)–(2.20). Moreover, in the limit $h_0 = 0$, $A_i = 0$ for $i = 1$, 2 and 3, $A_4 = A$ and $\eta_1 = 0$, equations (2.24)–(2.27) reduce to the usual system of equations governing van-der-Waals-driven rupture of a single layer in the presence of surfactant (Jensen & Grotberg 1992). The '0' subscripts are henceforth dropped on h_0, $\bar{h}_0$ and Γ_0; we retain the subscript on u_0 to emphasize that this is the surface velocity.

Equations (2.19)–(2.20) and (2.24)–(2.27) are solved numerically for a wide range of parameter values. In § 3, however, we shall look at similarity scalings and solutions for these equations in certain limits. These solutions will provide suitable limiting cases with which the numerical solutions can be validated.

3. Similarity solutions

Here, we derive similarity scalings for equations (2.19)–(2.20) and (2.24)–(2.27).

3.1. *Negligible van der Waals forces*

It is evident that in the low-diffusion limit, $Pe \to \infty$, the single-layer evolution equations (Jensen & Grotberg 1992; Jensen 1994) and the bilayer evolution equations where the mucus viscosity is of order one (Paper I) admit similarity solutions. Similarity solutions also exist for the bilayer case considered in the present work, where the mucus viscosity has been promoted. The analysis required is in essence similar to that of Jensen & Grothberg (1992), Jensen (1994) and Paper I, and a brief description of these scalings follows. The similarity solutions will be compared, at least for long times, with the full numerical solutions in § 4.

Substitution of the similarity variables

$$\xi = \frac{x}{\xi_s t^\alpha}, \quad h(x,t) = \frac{H(\xi)}{t^\beta}, \quad \bar{h}(x,t) = \frac{\mathrm{D}(\xi)}{t^\beta}, \quad \Gamma(x,t) = \frac{\xi_s^2 G(\xi)}{t^\gamma}, \quad u_0(x,t) = \frac{\xi_s U(\xi)}{t^\zeta}, \tag{3.1}$$

into equations (2.19)–(2.20) yields

$$\beta H + \alpha\xi H_\xi = \frac{1}{t^{\alpha+\zeta-1}}\left[U\left(H - \frac{\mathrm{D}}{2}\right)\right]_\xi = 0, \quad \beta \mathrm{D} + \alpha\xi \mathrm{D}_\xi = \frac{1}{t^{\alpha+\zeta-1}}\left[\frac{U\mathrm{D}}{2}\right]_\xi, \tag{3.2}$$

$$\gamma G + \alpha\xi G_\xi = \frac{1}{t^{\alpha+\zeta-1}}[UG]_\xi, \tag{3.3}$$

$$U = \mathrm{D}\left[\frac{\eta_1}{\xi_s^2 t^{2(\alpha+\beta)}}\{4(H-\mathrm{D})(\partial_\xi U)_\xi + 2(H-\mathrm{D})_\xi(U_\xi + \partial_\xi U)\} - \frac{1}{t^{\alpha+\beta+\gamma-\zeta}}G_\xi\right], \tag{3.4}$$

where the spreading exponents α, β, γ and ζ are to be found; ξ_s is a scaling factor to place the advancing front at $\xi = 1$.

There are two different cases to examine: $\beta \neq 0$ and $\beta = 0$; in the latter case we would expect the heights of the travelling peaks to remain approximately constant in time.

3.1.1. $\beta \neq 0$

Demanding that $\beta = -\alpha$, $\gamma = 1 - \alpha$, $\zeta = 1 - \alpha$, the equations become self-similar and the spreading rate α can then be found from the rate at which surfactant is supplied into the system; we use α_s to describe this latter rate. Let $Q(t)$ be the mass of surfactant, and Q_0 be the initial mass of surfactant present in the system at $t = 0$, then

$$Q(t) = Q_0 t^{\alpha_s} = \int_0^\infty \Gamma(x,t)\,\mathrm{d}x = \xi_s^3 t^{\alpha-\gamma}\int_0^\infty G\,\mathrm{d}\xi. \tag{3.5}$$

Thus we find $\gamma = \alpha - \alpha_s$, and hence

$$\alpha = -\beta = \frac{1+\alpha_s}{2}, \quad \gamma = \zeta = \frac{1-\alpha_s}{2}. \tag{3.6}$$

A general analytical solution of (3.2)–(3.4) is apparently unavailable. Such a solution, however, can be obtained for the case of a large viscosity contrast, η_1, between the mucus and PCL layers and a finite amount of surfactant ($\alpha_s = 0$). An equation for the thickness of the mucus layer, $\Delta = H - \mathrm{D}$, is obtained from equation (3.2): $\Delta - \xi\Delta_\xi + 2(U\Delta)_\xi = 0$. For large η_1, several terms decouple from (3.4), which simplifies to $\Delta U_\xi = 0$ after using the conditions ahead of the surfactant leading edge. This then leads to

$$U = \frac{\xi}{2}, \quad \Delta = 0, \tag{3.7}$$

for $\xi < 1$. Equation (3.7), and the associated scalings, will be used to validate the numerical solutions of the governing equations in the limit of large η_1, which will be presented in the following section. In particular, it will be shown that in planar geometry, the predicted $t^{1/2}$ scaling is in fact captured by the numerical simulations. (Similarly, we have verified that the axisymmetric scalings, $t^{1/3}$, are also recovered.)

3.1.2. $\beta = 0$

Here we assume that $\beta = 0$, that is, we expect the height scaling of the evolving pulses to remain constant with increasing time. Demanding $\zeta = 1 - \alpha$, $\zeta = \gamma + \alpha$ and using surfactant mass conservation, so $\alpha_s = \alpha - \gamma$, yields the scaling exponents as

$$\alpha = \frac{1+\alpha_s}{3}, \quad \gamma = \frac{1-2\alpha_s}{3}, \quad \zeta = \frac{2-\alpha_s}{3}. \tag{3.8}$$

Clearly in the case $\eta_1 \sim O(\epsilon^2)$ we recover the similarity scalings derived in Paper I

for the case of a Newtonian bilayer with the upper layer having a high yield stress. This restraining upper high-yield-stress layer has some physical similarities with the highly viscous skin; both prevent shear in the layer. For larger η_1 the variables take so long to evolve to the similarity scalings that they appear to follow another scaling. For either long times, or for bilayers without such large viscosity mismatch, the following similarity solutions are obtained:

$$\left.\begin{aligned} H(\xi) &= (1-\delta_0)[2\xi\Theta(1-\xi)+1-\Theta(1-\xi)]+\delta_0\Theta'(1-\xi),\\ \mathrm{D}(\xi) &= (1-\delta_0)[2\xi\Theta(1-\xi)+1-\Theta(1-\xi)],\\ G(\xi) &= \frac{\alpha(1-\xi)}{2(1-\delta_0)}\Theta(1-\xi), \quad U(\xi) = \alpha\xi\Theta(1-\xi), \end{aligned}\right\} \tag{3.9}$$

where Θ is the Heaviside step function, and its derivative, Θ', is the Dirac-delta function. Here δ_0 is the initial mucus layer thickness, and the scaling constant, ξ_s, is given by

$$\xi_s = [12Q_0(1-\delta_0)]^{1/3}, \tag{3.10}$$

in which $Q_0 = \sqrt{\pi}/2$ in the numerical solutions. (In axisymmetric geometry, $\xi_s = [16Q_0(1-\delta_0)]^{1/4}$ with $Q_0 = 1/2$.) The solution for $\mathrm{D}(\xi)$ is compared with numerical simulations in § 4.

3.2. *Significant van der Waals forces*

In the presence of van der Waals forces, (2.24)–(2.27) can be recast in terms of the following similarity variables:

$$\xi = \frac{x-x_\mathrm{r}}{(t_\mathrm{r}-t)^\alpha}, \quad h(x,t) = \frac{H(\xi,\tau)}{(t_\mathrm{r}-t)^\beta}, \quad h-\bar{h}(x,t) = \frac{\Delta(\xi,\tau)}{(t_\mathrm{r}-t)^\varpi},$$

$$\Gamma(x,t) = \frac{G(\xi,\tau)}{(t_\mathrm{r}-t)^\gamma}, \quad u_0(x,t) = \frac{U(\xi,\tau)}{(t_\mathrm{r}-t)^\zeta}, \tag{3.11}$$

where $\tau = t_\mathrm{r}-t$. For a thin mucus film, with all the Hamaker constants non-zero, there are two modes of rupture: the mucus film itself ruptures with the PCL remaining intact, or the PCL and mucus simultaneously approach the base and effectively rupture together.

The former occurs for small η_1 where the mucus layer provides less resistance to rupture, and the latter for large η_1. In this latter case assuming that $h, \bar{h}$ scale identically and that van der Waals, capillarity and viscous forces balance then the simpler, single-layer limit scalings are recovered, that is, $\alpha = 2/5$, $\beta = -1/5$ (Zhang & Lister 1999*b*) and $\gamma = -3/10$ (Warner, Craster & Matar 2002), the scalings for ζ and ϖ appear, from later numerical results, to be 1 and $-3/10$ respectively.

When the mucus alone ruptures, we assume that $\bar{h}$ is approximately constant and that the dominant terms are associated with the van der Waals forces within the film, and the capillarity and longitudinal stresses there. If this is the case, then one obtains $\zeta \sim 5/6$, $\alpha \sim 1/6$, $\varpi \sim -1/3$ and $\beta \sim -1/12$, the surfactant becomes enslaved to the mucus thickness and $\gamma \sim -1/3$. These scalings will be compared with numerical simulations.

4. Numerical results

In this section, we present numerical solutions of the evolution equations (2.19)–(2.20) and (2.24)–(2.27) for a wide range of system parameters, and compare them

with the similarity solutions/scalings. We begin by providing some details of the numerical schemes employed to carry out the computations.

4.1. *Solution procedure*

The numerical scheme primarily utilized is a PDE solver, EPDCOL (Sincovec & Madsen 1979; Keast & Muir 1991), a highly efficient and versatile code designed for the solution of systems of nonlinear parabolic equations. It is based upon finite-element collocation in the spatial coordinate and the method of lines approach for time. Further checks on the accuracy of the numerical computations were performed using an adaptive grid scheme, Blom & Zegeling (1994), as well as finite-difference schemes (Matar & Troian 1999*a*, *b*). Typically 2000 grid points were employed on a computational domain of length 30 dimensionless units, although this had to be extended to 40 units in the case of large-η_1 simulations (see below). The results of our simulations were in excellent agreement with earlier published results for spreading on Newtonian (Jensen & Grotberg 1992) and non-Newtonian single and bilayers (Paper I). Our numerical solutions are also compared with the predictions of the similarity solutions derived analytically in § 3.

Spreading is forced by the following initial conditions:

$$h(x,0) = 1, \quad \mathrm{d}(x,0) = \bar{h}_0 < 1, \quad \Gamma(x,0) = \exp(-x^2), \quad u_0(x,0) = 0, \tag{4.1}$$

where $\bar{h}_0$ is a constant height with $0 < \bar{h}_0 < 1$. Initial conditions for the surfactant concentration, which are similar in form to (4.1), have previously been used to provide a smooth approximation to the concentration within a monolayer (Jensen & Grotberg 1992; Matar & Troian 1998; Matar & Troian 1999*a*; Paper I).

Numerical solutions are obtained subject to the following set of boundary conditions:

$$\left.\begin{array}{l} h_x = \bar{h}_x = \Gamma_x = u_0 = 0 \quad \text{at} \quad x = 0; \\ h = 1, \quad \bar{h} = \bar{h}_0, \quad \Gamma = 0, \quad u_0 = 0 \quad \text{as} \quad x \to \infty. \end{array}\right\} \tag{4.2}$$

These conditions represent no flux of surfactant and symmetry at the flow origin, and the recovery of undisturbed conditions far from the original point of surfactant deposition located at the origin.

Solutions are obtained for the range $0.1 \leqslant \eta_1 \leqslant 100$ and, unless otherwise stated, for $\delta_0 = 0.1$. Computations are performed for times $t = 40$–10^4. These values are chosen to be long enough to enable comparisons with the self-similar solutions. The Péclet number is fixed to be $Pe = 1000$ in line with the order-of-magnitude estimates (table 2 of Paper I), which corresponds to a primarily Marangoni-driven spreading process, while lower values are not representative of typical spreading conditions. Perhaps surprisingly, larger values of Pe do not lead to the rapidly varying spatial derivatives seen in previous studies, since here the skin serves to smooth out these shock-like features. The only real effect of increasing Pe in the range $Pe > 1000$ is that the heights of the mucus peaks in the advancing front are marginally increased, and their widths are slightly narrowed.

Within all the numerical results we define the 'front position' to be that where the fluid layer attains its maximum, $h = h_{\max}$.

4.2. *Negligible van der Waals forces*

Numerical solutions of the equations governing spreading in the absence of van der Waals forces are presented first.

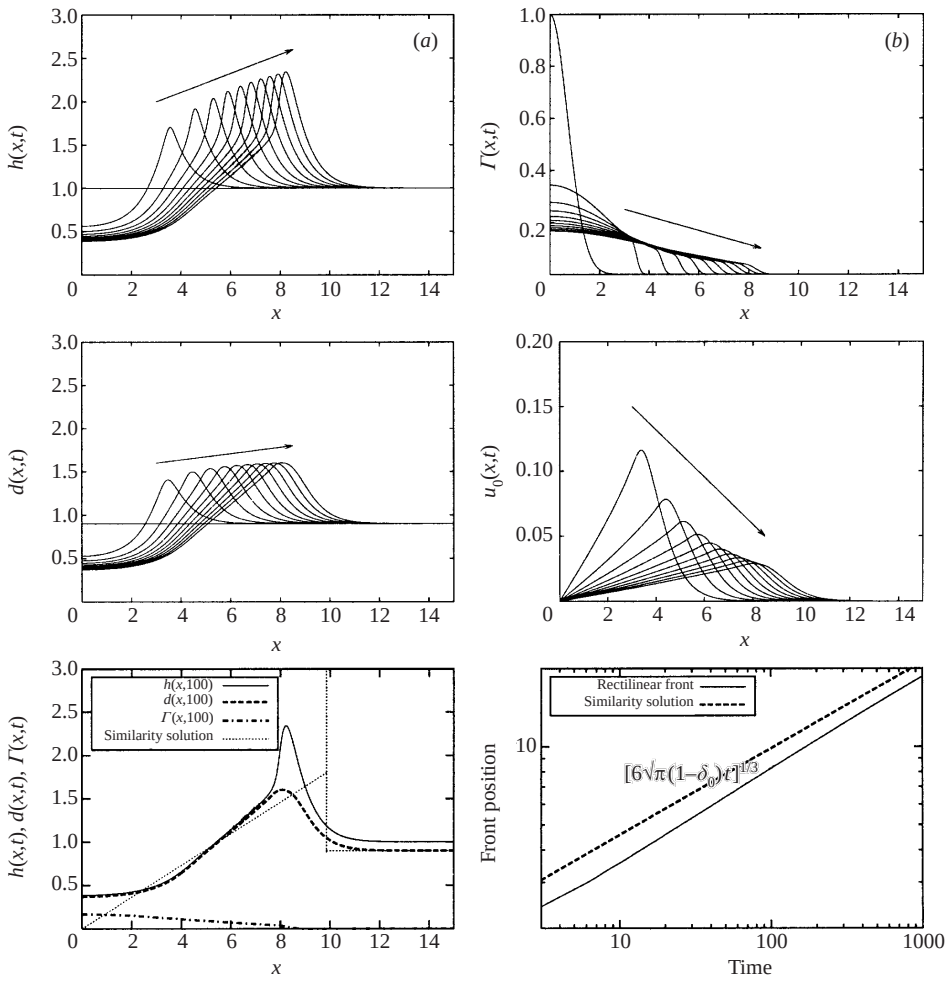

FIGURE 1. Typical evolution for $t = 0$ to 100 in steps of 10 time units, the arrow showing increasing time. The parameter values are: $\eta_1 = 1$, $Pe = 1000$ and $\delta_0 = 1/10$. The dotted line in (e) shows the similarity solution for $\bar{h}(x,t)$ valid for small η_1.

4.2.1. *Typical simulation*

Figure 1 shows the spatio-temporal evolution of h, d, Γ and u_0 for $Pe = 1000$, $\eta_1 = 1$ and $\delta_0 = 0.1$, typical parameter values. The spreading process is accompanied by large deformations in the underlying bilayer: rapid and severe thinning near the original surfactant deposition at the flow origin and upwelling of the fluid bilayer at the surfactant leading edge. These upwellings are particularly pronounced for the mucus layer, assuming the form of propagating pulse-like structures, compared with the thickened fronts in the underlying PCL layer. Close inspection of the concentration profiles does not reveal monotonic decrease but rather considerable steepening of the profiles into fronts at the surfactant leading edge immediately preceded by shallow minima; this is markedly different to the behaviour of the single layer (Jensen & Grotberg 1992) and previously studied bilayer cases (Paper I). These sharp fronts seem to coincide with the peaks in the mucus and PCL layers as well as the maxima in the velocity profiles. Inspection of the height and velocity profiles reveals that

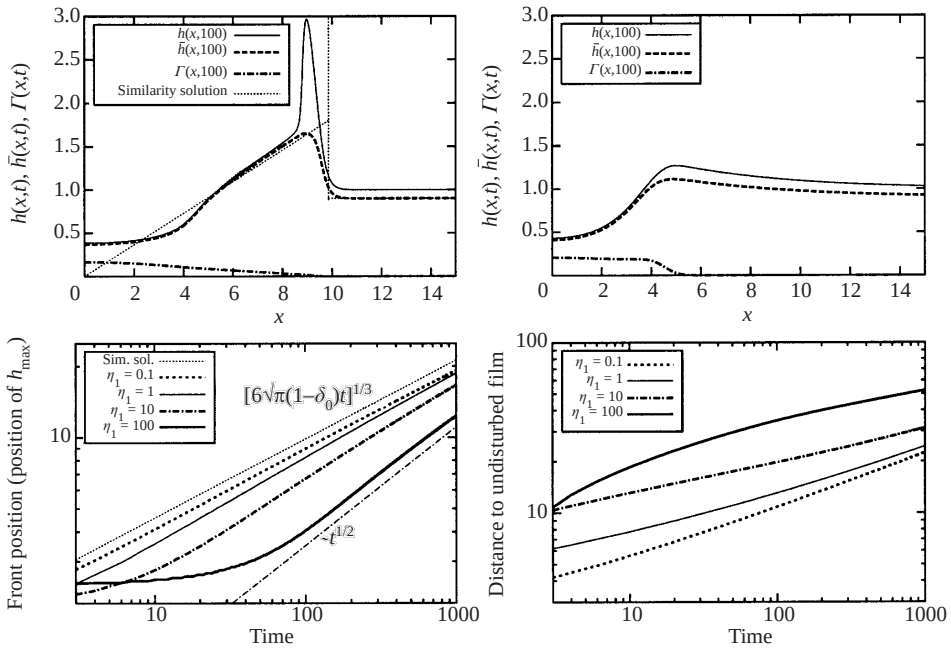

FIGURE 2. The effect of η_1 on the flow characteristics; the other parameter values are $Pe = 1000$ and $\delta_0 = 0.1$. The similarity solution for $\bar{h}(x,t)$, valid for small η_1, is also shown.

undisturbed conditions are recovered a relatively large distance downstream from the surfactant leading edge. As the spreading evolves, gradients in the surfactant concentrations decrease in magnitude due to dilution, as does the velocity in the mucus layer.

It is notable that shock-like, rapidly varying, solutions might invalidate the lubrication approximation, and some care is required in the interpretation; the pulse-like structures have a characteristic width proportional to t^{α} and so lengthen over time; additionally surface diffusion, and in the present case the action of the mucus film, act to smooth out very rapid variations.

Figure 1 also shows that numerical solutions and similarity scalings compare favourably over a large proportion of the domain, with the exception of a narrow region near the flow origin in which the numerical solutions must match the imposed no-flux and symmetry boundary conditions. This agreement is also reflected in the comparison of the numerically generated position of the front with that predicted by the similarity scalings. We shall revisit this comparison in the following subsections in which we discuss the effect of η_1 on the dynamics.

4.2.2. *The effect of varying* η_1

Figure 2 shows the effect of varying the mucus viscosity on the flow profiles and spreading rates. An increase in the viscosity gives rise to less pronounced, smoother fronts in the mucus and PCL which decay spatially over large distances as well as steeper surfactant concentration profiles. The latter feature is presumably brought about by the increase in viscous retardation of the spreading, while the former is due to the increasingly viscous skin becoming more resistant to deformations. As expected, the agreement of the numerical solutions with the similarity solution for $\bar{h}(x,t)$ improves with decreasing η_1, becoming quite good for $\eta_1 = 0.1$ with the

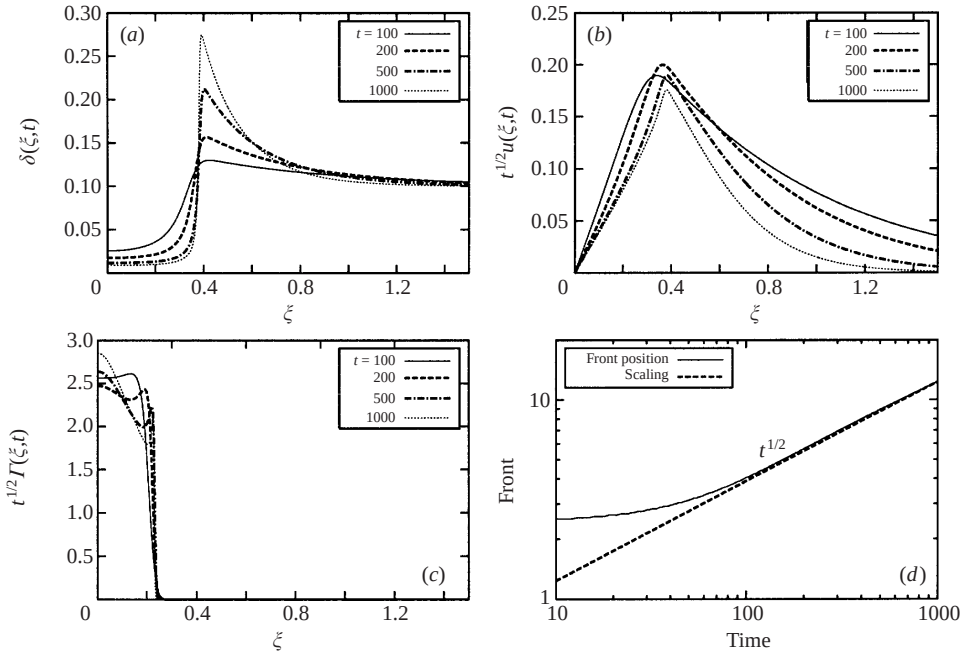

FIGURE 3. Large-η_1 dynamics for $t = 100$, 200, 500, 1000. (a) δ, (b) u and (c, d) spreading rates, with $\delta_0 = 0.1$, $Pe = 1000$ and $\eta_1 = 100$.

exception, once again, of the narrow boundary layer region near the flow origin at which the solutions must match $h_x = \bar{h}_x = \Gamma_x = 0$.

As can be seen upon inspection of figure 2(c, d), the spreading rates also begin to diverge from those predicted by the small-η_1 similarity scalings with increasing η_1. In fact, it appears as though another power-law spreading regime is approached for large η_1.

In order to investigate that regime we focus on the dynamics of spreading on very highly viscous skins, shown in figure 3 for times up to $t = 1000$, characterized by $\eta_1 = 100$ with all other parameters unaltered from figure 2. Despite the large magnitude of η_1, the mucus layer is flat near the flow origin and forms a large spike at the surfactant leading edge, the magnitude of which increases with time; this structure exhibits very slow spatial decay to undisturbed conditions far downstream of the spreading monolayer. The magnitude of the velocity, however, which is greatly reduced in comparison with that in figure 1 in which $\eta_1 = 1$, as expected, decreases with increasing time. Figure 3(d), which also shows the large difference between the location at which undisturbed conditions are recovered and that of the maximum in the total height (coincident with the surfactant leading edge), reveals that spreading proceeds as $t^{1/2}$ for large η_1 compared to $t^{1/3}$ as is the case for small values of η_1. This is consistent with the similarity scalings in § 3.1.1.

4.2.3. *Comparison with highly viscous bilayers*

Here predictions of the highly viscous theory are compared with those for two Newtonian layers with differing viscosities, both of the same order of magnitude (Paper I). As a brief summary from this previous work the horizontal velocities

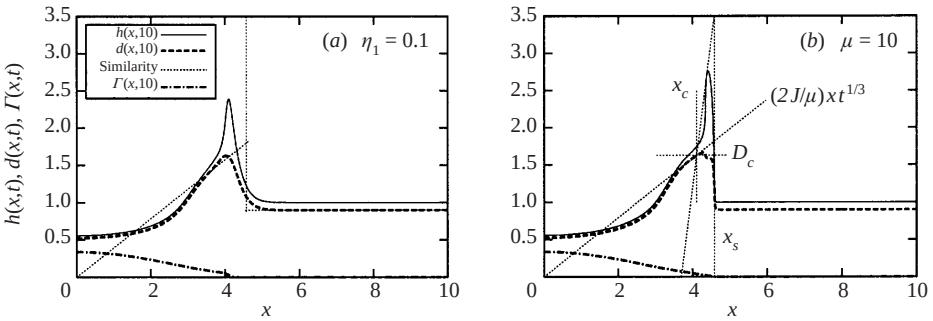

FIGURE 4. The highly viscous film theory (a) versus the standard lubrication theory for a bilayer (b). (a) $\delta_0 = 0.1$, $Pe = 1000$ and $\eta_1 = 0.1$. (b) $Pe = 1000$, a mucus to PCL thickness ratio of 0.1 and a viscosity ratio of 10. The similarity solutions are shown as dot-dash lines. Also shown in (b) is the prediction of the second 'shock' position, ξ_c. The lines are labelled as follows: $x_c = \xi_c t^{1/3}$, $x_s = \xi_s t^{1/3}$, $\bar{H}_c = 2(J_-/\mu)[1 - (-\mu\bar{h}_0/J_-)^{1/2}]$.

within each layer in this limit are given by

$$u(x,z,t) = \frac{\sigma_x}{\eta_1}(z - \bar{h}) + \bar{h}\sigma_x \quad \text{for} \quad \bar{h} < z < h, \quad \bar{u}(x,z,t) = \sigma_x z \quad \text{for} \quad 0 < z < \bar{h}, \tag{4.3}$$

where the mucus viscosity, $\hat{\eta} = \eta_1\eta_0$, is no longer promoted by the division by ϵ^2, and the PCL viscosity remains unity. This comparison, where η_1 in the 'skin' theory is small so that the longitudinal stress terms play a smaller role is shown in figure 4. It reveals good agreement between the two theories, with the majority of the discrepancies being confined to the details of the mucus and PCL peaks in a narrow region at the surfactant leading edge. Notably absent from the highly viscous theory profiles is the small shock-like peak that adjusts onto a flat solution in the PCL profile just after the major shock-like structure, which is a feature of the standard lubrication predictions (Paper I); this secondary shock-like feature is apparently suppressed by the presence of the skin. Recovery of undisturbed conditions occurs further downstream from the surfactant leading edge in the skin case than in standard lubrication. This is presumably due to the influence of the 'stretching' terms proportional to $\eta_1 u_{0xx}$, which have been promoted in the highly viscous theory but are absent from standard lubrication. This feature is accentuated by increasing η_1 as was demonstrated in figure 2, and the results for the two theories diverge.

The bilayer theory has a small secondary feature in the PCL solution. This is located at the position where the similarity solution, $D(\xi)$ in Paper I, reverts from the solution proportional to ξ valid at $\xi = 0$, to the constant solution valid at the shock, $\xi = 1$, and thus where the secondary shock-like feature occurs. If we call this position ξ_c, and require conservation of volume, then, in the notation of Paper I we have

$$\int_0^{\xi_c} \frac{2J_-}{\mu^{1/n}}\xi \mathrm{d}\xi + \int_{\xi_c}^1 \frac{2J_-}{\mu^{1/n}}\left(1 - \sqrt{1 - \frac{\mu^{1/n}\bar{h}_0}{J_-}}\right)\mathrm{d}\xi = \bar{h}_0, \tag{4.4}$$

and hence

$$\xi_c = \left(1 - \sqrt{1 - \frac{\mu^{1/n}\bar{h}_0}{J_-}}\right).$$

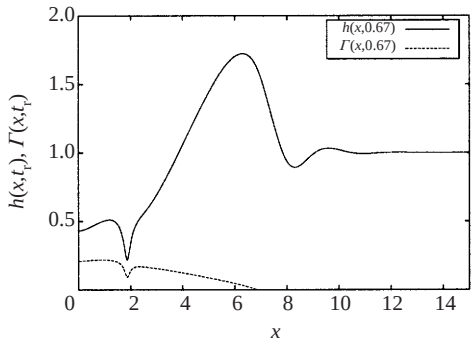

FIGURE 5. Spreading of a single Newtonian layer in the presence of van der Waals and capillary forces. Parameter values: $\mathscr{M} = 50$, $Pe = 1000$, $\mathscr{A} = 1$.

Here $J_- = [1 + (\mu^{1/n} - 1)\bar{h}_0]$ in which n is the flow index (equal to unity in the present case), μ is the viscosity contrast between the mucus and PCL layers (equivalent to η_1/ϵ^2 here) and $\bar{h}_0$ is the initial PCL depth. Equation (4.4) simply shows that the similarity solutions must remain continuous at this second shock position, and hence this blip should not appear when the solution has evolved sufficiently to become self-similar. Nevertheless, this small shock is a feature of the numerical solutions (and appears, at least, to coincide with the predicted value of ξ_c). This, therefore, leads us to conclude that it is a consequence of requiring the zero-gradient boundary conditions at $\xi = 0$; this can be seen from figure 4, where near $x = 0$ in the numerical solution there is a small amount of 'excess' mass which accumulates at the shock.

4.3. *Significant van der Waals forces*

In this section we present results from numerical simulations of the spreading process driven by Marangoni stresses, and van der Waals and capillary forces; a typical flow profile of a monolayer spreading on a single viscous film is shown in figure 5. The introduction of van der Waals force leads to an instability developing behind the frontal travelling pulse, causing the thinning in this region to become much more severe, and ultimately film rupture to occur. As noted earlier this could have serious implications for surfactant delivery: film rupture could lead to quantities of surfactant remaining trapped. Incidentally, the introduction of capillary forces leads to a small-amplitude wave travelling ahead of the main shock-like feature.

The same numerical procedures employed to obtain the results in the absence of van der Waals forces are also used here; the initial and boundary conditions also remain unaltered. We investigate the effect of the presence of a highly viscous mucus skin on the possibility of bilayer rupture for the following range of system parameters: $0.1 \leqslant \eta_1 \leqslant 10$, $5 \leqslant \mathscr{M} \leqslant 100$, $0.05 \leqslant \delta_0 = 1 - \bar{h}_0 \leqslant 0.3$, $0.001 \leqslant A_2 \leqslant 0.1$, with $Pe = 1000$ held constant as in the previous simulations. It proved very difficult to carry the computations to the final stages of rupture since the spatial derivatives become increasingly singular and consequently more difficult to resolve as rupture is approached. In all cases considered, the computations were therefore halted when the thickness of the mucus layer in the rupture region is at most $O(10^{-3})$, which yielded an estimate of the rupture time.

4.3.1. *Typical simulation*

The evolution of the spreading process including van der Waals and capillary forces, shown in figure 6 for $\mathscr{M} = 50$, $\eta_1 = 1$, $\delta_0 = 0.1$, $A_1 = A_3 = A_4 = 1$, $A_2 = 0.01$

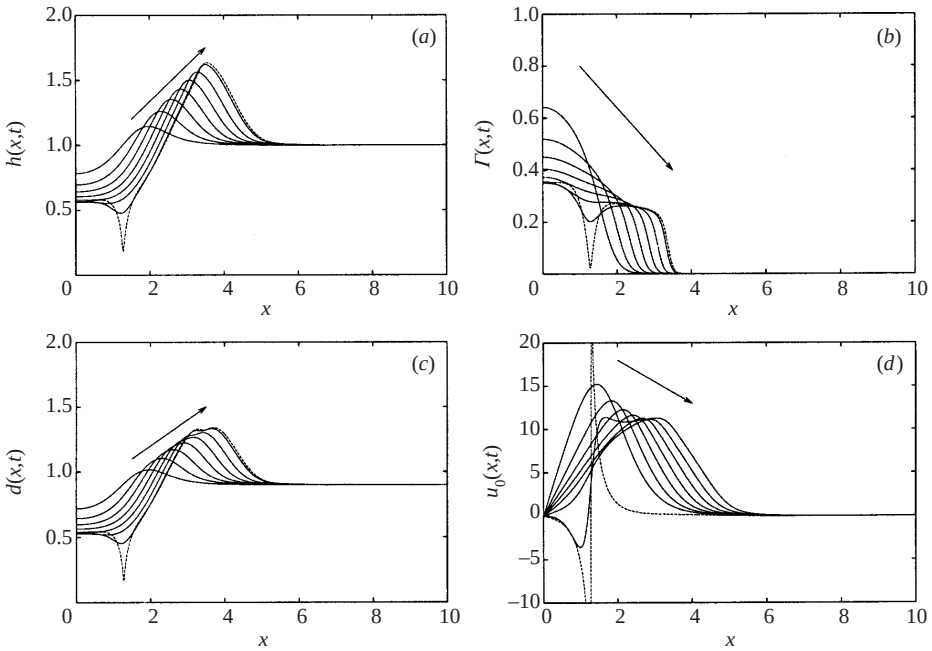

FIGURE 6. Evolution of the spreading process including van der Waals and capillary forces at $t = 0.02$, 0.04, 0.08, 0.1, 0.12, 0.14 and $t_r \approx 0.144502$, the arrow indicating increasing time, with $\eta_1 = 1$, $Pe = 1000$, $\mathscr{M} = 50$, $\delta_0 = 0.1$, $A_1 = A_3 = A_4 = 1$ and $A_2 = 0.01$. The dotted line shows a solution close to the rupture time. (In the case of (d) the dotted line shows $u_0/100$.)

and $Pe = 1000$, is similar to that presented in figure 1: the formation of a thickened front in both the mucus and PCL layers, which extends far downstream of the steep concentration profiles at the surfactant leading edge is also evident here. After a certain period of time, which is dependent on the chosen parameter values and initial surfactant concentration profile, the film begins to thin near the flow origin and a rupture instability begins to develop.

The flow giving rise to this thinning advects surfactant away from the rupture region, as revealed by inspection of the velocity profile in figure 6(d), which undergoes an abrupt change in sign at the rupture point; this leads to local surfactant depletion. The magnitude of the velocity near rupture is large, which is indicative of the strength of this flow. The magnitude of the van der Waals forces, which are responsible for this rupture instability, increases below the thinning region leading to further advection of surfactant from that region. This gives rise to gradients in surfactant concentration and hence Marangoni stresses that drive flow back towards the rupture region, which act to stabilize the bilayer against rupture. In this case, the potentially stabilizing effect of surfactant is insufficient to prevent rupture, which occurs at $t \approx 0.144502$ for the simulation shown.

The PCL thickness profile exhibits an interesting feature: some minor local thinning at the peak of the PCL thickened front, more evident in figure 2; this feature is absent from the mucus height profile. The physical mechanism for this thinning is unclear: why does the PCL front undergo rupture since intermolecular forces, which are presumably responsible for the thinning, should be insignificant near the front? This phenomenon, which is spatially coincident with the advancing surfactant front and present even in the absence of van der Waals forces (see figure 7), may be correlated

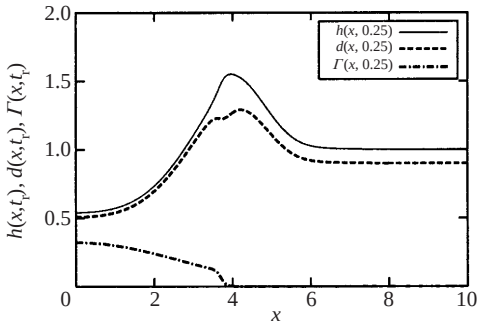

FIGURE 7. Simulations with all Hamaker constants equal to zero showing the thinning phenomenon in the PCL peak. The remaining parameters are unchanged from figure 6.

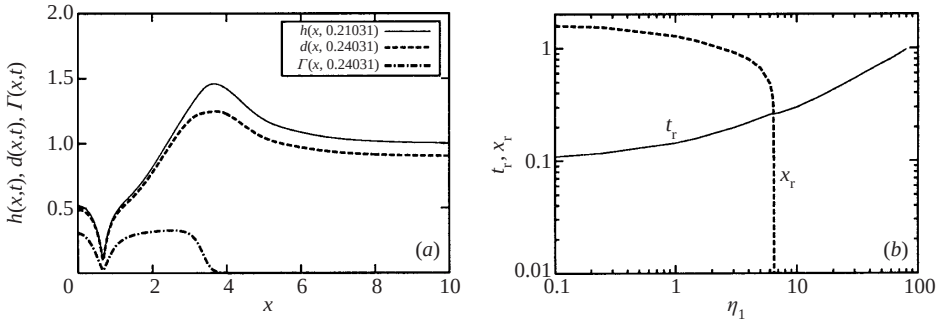

FIGURE 8. The effect of η_1 on bilayer rupture. (*a*) $\eta_1 = 5$, (*b*) variation of t_r and x_r with η_1; the remaining parameters are unchanged from figure 6.

with the shape of these fronts, which are steep step-like profiles and no longer slowly and smoothly varying as shown in figures 1 and 2.

We have also studied the effect of varying A_i on the rupture dynamics. Our results (not shown) indicate that the term A_2/d^3 provides the dominant contribution. Increasing A_2 while keeping all other parameters constant leads to a decrease in the rupture time, t_r, and rupture location, x_r.

4.3.2. *Varying the mucus viscosity*

Here we investigate the effect of increasing the skin viscosity, η_1, on the rupture dynamics. Figure 8 shows the total height, the PCL thickness and surfactant concentration profiles shortly before rupture for $\eta_1 = 5$ and the effect of η_1 on t_r and x_r. With increasing mucus viscosity, η_1, appears to retard the rupture instability and displace the rupture point closer to the flow origin. This is not unexpected, since observation of the evolution equation for u_0, equation (2.24), reveals the importance of the quantity $\mathscr{M}/\eta_1$, which governs the ratio of Marangoni stress to the other forces. In effect increasing η_1 (or equivalently decreasing $\mathscr{M}$), reduces the ratio of Marangoni forces, thereby reducing the rupture position, x_r. Increasing η_1 also appears to retard and, for sufficiently large values of η_1, prevent the local thinning at the front in the PCL layer seen for small values of η_1 (see figure 7).

Also evident with increasing η_1 is the substantial film height disturbance that occurs further downstream than for less viscous skins. This causes potential numerical problems for highly viscous mucus layers, as the computational spatial grid must be

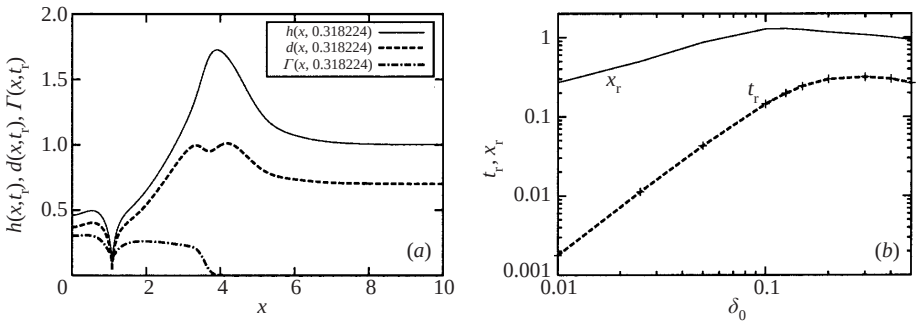

FIGURE 9. The effect of δ_0 on bilayer rupture. (*a*) $\delta_0 = 0.3$, (*b*) variation of t_r and x_r with δ. The rest of the parameter values remain unchanged from figure 6.

significantly extended, with the result that accuracy is lost in the rupture region; because of this problem very highly viscous films are not considered here.

4.3.3. *Varying the initial mucus layer thickness*

Here we investigate the effect of varying the initial depth of the mucus layer δ_0. Figure 9 shows the total height, the PCL thickness and surfactant concentration profiles shortly before rupture for varying values of $\delta_0 = 3$ and the effect of δ_0 on t_r and x_r. Comparison of figure 6 and figure 9 shows that an increase in the mucus layer depth appears to significantly increase the time to the initial rupture of the films, whilst accentuating the local thinning of the PCL layer within the advancing peak. However, despite the increased time to the rupture event the actual position of the rupture is displaced further towards the origin with increasing mucus thickness beyond the value of $\delta_0 = 0.1$. This is perhaps not unexpected as the highly viscous mucus layer serves to retard the spreading Marangoni effects as well as the attractive intermolecular van der Waals force. However, inspection of figure 9 shows that t_r and x_r do not depend monotonically on δ_0. This, therefore, leads to the conclusion that there is a critical initial mucus layer depth, δ_{0c} say, which causes the greatest mass of the surfactant to become trapped and is therefore most detrimental to the process of chemical delivery. For instance, in the case shown in figure 9, δ_{0c} appears to have an approximate value of 0.1.

To further investigate this transition at $\delta_0 \sim 0.1$ a linear stability analysis of a uniform base state with $u_0 = 0$, $h = 1$, $\bar{h} = 1 - \delta_0$ and $\Gamma = 1$ was performed. The variation of the wavenumber corresponding to the most dangerous mode, k_m, and the associated maximal growth rate, λ_m, with skin thickness is shown in figure 10; although the stability analysis is for a different base state, a flat film, one can show connections with the numerical results. Both graphs have a minimum near $\delta_0 = 0.1$; in the case of k_m this means the unstable wavelength is largest there and so x_r should be maximized; for λ_m, the maximal growth rate is smallest there and effectively means we should have a longer time to rupture, hence t_r is maximized.

4.3.4. *The effect of varying the Marangoni parameter, $\mathcal{M}$*

Here we investigate the effect of changing the Marangoni number, $\mathcal{M}$, to 100 and the effect of $\mathcal{M}$ on t_r and x_r. Figure 11 shows the total height, the PCL thickness and surfactant concentration profiles shortly before rupture for varying values of $\mathcal{M}$. Increasing the Marangoni number has the effect of increasing the displacement of the rupture position from the origin, whilst at the same time reducing the time taken

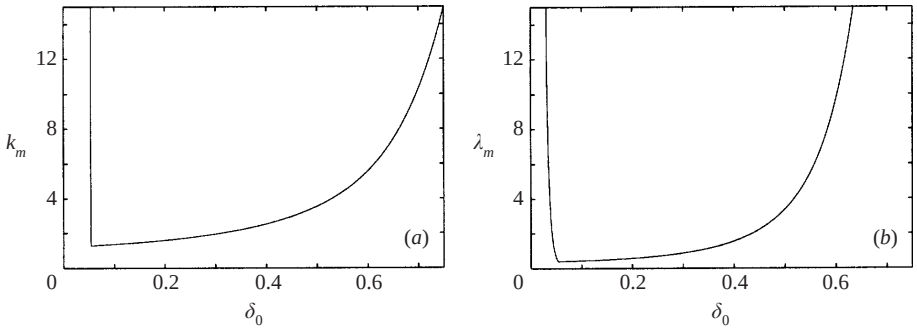

FIGURE 10. The wavenumber corresponding to the most dangerous mode, k_m, and the associated maximal growth rate, λ_m, versus initial skin thickness, δ_0, as determined from a linear stability analysis.

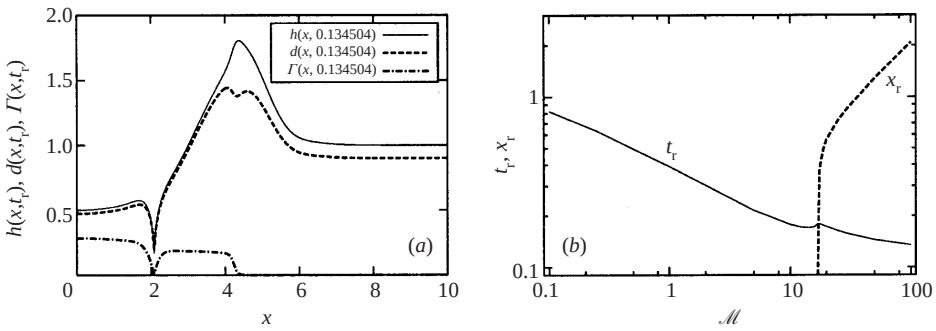

FIGURE 11. The effect of $\mathscr{M}$ on bilayer rupture. (*a*) $\mathscr{M} = 100$, (*b*) variation of t_r and x_r with $\mathscr{M}$. The rest of the parameter values remain unchanged from figure 6.

for the bilayer system to rupture. Despite the fact that in general we would expect the Marangoni force to be a stabilizing one, it is clearly seen that increasing $\mathscr{M}$ significantly leads to a faster rupture. This can be explained by the fact that when $\mathscr{M}$ is large, we have a situation with fast spreading, and therefore very rapid thinning of the mucus behind the propagating peak. This very much thinner layer is then more sensitive to the rupture instability (as observed in the previous section), and so rupture time is reduced. Inspection of these flow profiles also shows that an increase in the magnitude of Marangoni effects is another factor that leads to the exaggeration of the local thinning of the PCL layer within the advancing peak. For low Marangoni numbers, $0 \leqslant \mathscr{M} \leqslant 10$, rupture occurred at the origin, and therefore no surfactant became trapped. However, it should also be noted at this point that as the Marangoni number decreases in magnitude the scaling $\mathscr{S} \sim \epsilon^2 s$ becomes invalid, and we will recover that $\mathscr{M} \sim \mathscr{S}$. In this case it is possible that surface tension gradients will affect capillarity and we would need to re-introduce the pressure as

$$p_0 = -\left(1 + \frac{\mathscr{S}\sigma}{\sigma_m}\right)\kappa, \quad \bar{p}_0 = -\left(1 + \frac{\bar{\mathscr{S}}\bar{\sigma}}{\bar{\sigma}_m}\right)\bar{\kappa},$$

where $\mathscr{S}$ is no longer negligible, to investigate this parameter range. Results from simulations with this redefined pressure (not shown) yielded minor quantitative differences.

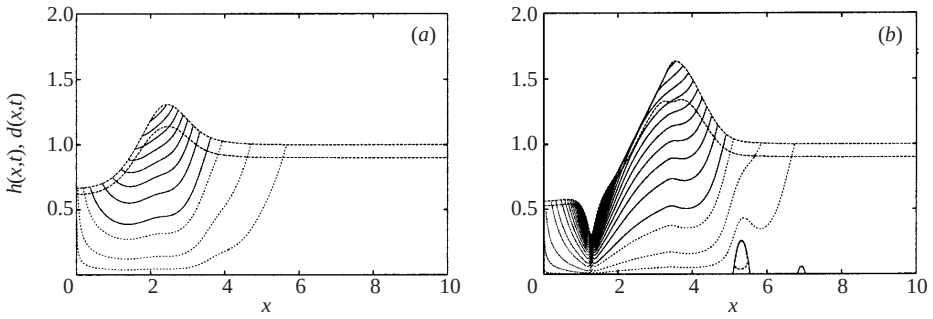

FIGURE 12. Streamlines for the rupture problem with parameter values: $\eta_1 = 1$, $\delta_0 = 0.1$, $\mathscr{M} = 50$, $Pe = 1000$, $A_1 = A_3 = A_4 = 1$ and $A_2 = 0.01$ at (*a*) $t = 0.05$, (*b*) 0.1444.

4.3.5. *Stream function*

In an effort to understand the precise motion of the flow within the fluid layer, we construct the stream function, ψ, where we define $(u_0, w_0) = (\psi_z, -\psi_x)$ in Cartesian rectilinear geometry.

The stream function within the PCL layer is

$$\bar{\psi} = \left[\frac{u_0}{\bar{h}} + \left(\frac{z}{3} - \frac{\bar{h}}{2}\right)(\bar{p}_0 + \bar{\phi})_x\right]\frac{z^2}{2}, \tag{4.5}$$

where h, $\bar{h}$, Γ, u_0 are available from numerical simulations; we have assumed that $\bar{\psi} = 0$ corresponds to the no-slip region at the base. Within the mucus layer the stream function is given by

$$\psi = -\frac{\bar{h}u_0}{2} - \frac{1}{12}\bar{h}^3(\bar{p}_0 + \bar{\phi}_0)_x + zu_0, \tag{4.6}$$

and it is easily seen that at the interface, $z = \bar{h}$, the stream function is continuous as must be required, $\psi = \bar{\psi}$. Comparison of figure 12 with similar plots for an insoluble surfactant monolayer spreading on a single layer (see for instance figure 1 in Jensen & Grotberg 1993) reveals that substantial activity occurs in the present case downstream of the surfactant fronts; this activity is absent in the monolayer case. This activity is due to the stresses in the mucus layer, which have been increased under our new scaling, being transmitted much further downstream than in the more usual limit.

With the introduction of van der Waals and capillary forces, shown in figure 12, the velocity field becomes substantially more complicated with several distinct regions of activity clearly evident. Initially the flow profile behaves in a similar manner to the simple spreading case with the addition of a noticeable downward deviation in the streamline paths coincident with the x-coordinate of the surfactant leading edge. This buckling of the streamlines becomes more exaggerated with increasing time, and at approximately $t \approx 0.1$ for the typical parameters, a vortex is shed below the leading edge of the upwelling in the fluid; this is separated from the rest of the flow region by the $\psi = 0$ streamline. Indeed a succession of vortices located ahead of the travelling peak seem to appear, before being swamped at the onset of rupture by the associated large velocity. However, for smaller values of η_1, where the usual capillary waves are not suppressed, as in this typical simulation, the vortices do not appear to arise. It is worthy of mention that work involving Stokes flow driven by surface tension gradients has also revealed the presence of Moffatt vortices ahead of the shock (Jensen & Halpern 1998).

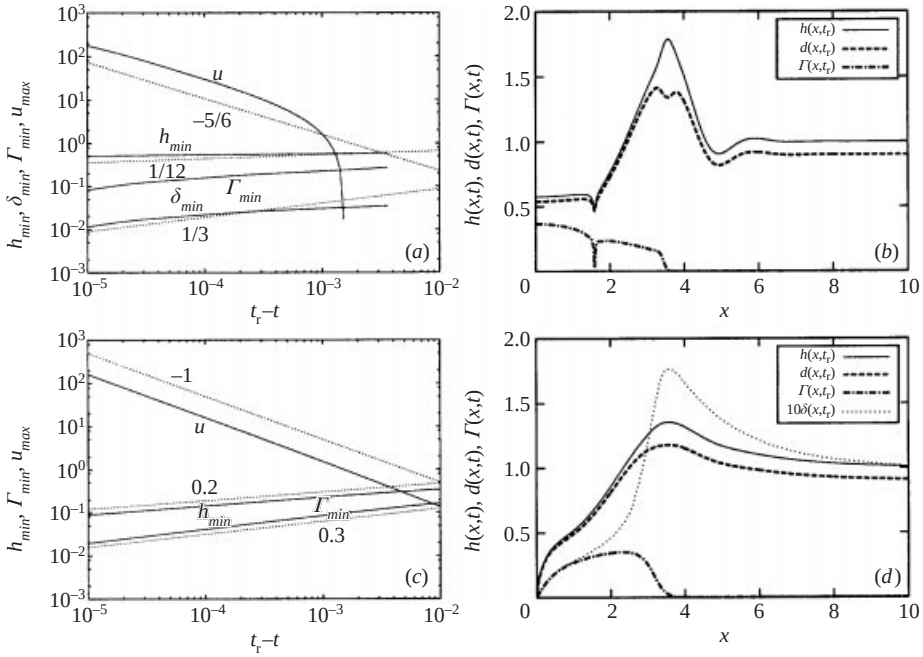

FIGURE 13. (a, b) The scalings and the final profile for the case $\eta_1 = 0.1$. In this case the mucus layer ruptures considerably before the PCL. (c, d) The scalings and the final profile for the case when $\eta_1 = 10$ where both layers appear to rupture almost simultaneously.

4.3.6. *Comparison with self-similar rupture scalings*

Near the rupture event we expect either the mucus alone to rupture, or both PCL and mucus to rupture together; as an aside, for very thick mucus films one can have the PCL rupturing first; however this seems irrelevant for the application considered here. Some sample numerical simulations are shown in figure 13. As mentioned earlier (§ 3.2), it is possible to deduce scalings near this rupture region and these are shown in figure 13 together with results from the simulations. It is particularly notable that the surfactant concentration decreases near rupture, and the Marangoni induced flow can retard the time to rupture but is unable to prevent rupture occurring.

5. Concluding remarks

Monolayer spreading of insoluble surfactant on the surface of a thin highly viscous Newtonian mucus layer, overlying an essentially watery Periciliary liquid layer (PCL), is considered here as a preliminary model for chemical transport along diseased, or surfactant depleted, airways in which the flow is driven primarily by Marangoni stresses. We have developed and investigated a model that allows large viscosity mismatches between the PCL and mucus. The model itself has connections with, and may have further applications in, other biomechanical flows such as particle motion in lipid membranes overlying less-viscous phases (Saffman 1976; see also § 3 of Stone 2000). It can also have an impact upon other physical modelling where the Boussinesq–Scriven surface viscosity theory is at present employed with surface tension forces. The strongly coupled system of four partial differential equations for the total film height, PCL thickness and surfactant interfacial concentration, and the horizontal velocity in the mucus layer is also reminiscent of models for free films and

jets (Erneux & Davis 1993; Papageorgiou 1995*a*, *b*) except that inertia plays no role in the present application.

An understanding of how the proposed model affects conclusions taken from conventional single-layer, or bilayer, Newtonian problems requires an investigation of the spreading process itself, and of possible rupture events. Although scenarios triggered by the deposition of a finite compact mass of surfactant are considered here, in the application to surfactant replacement therapy the model would have to be extended to deal with complex lung geometry; recently, models have emerged for this with spreading along a single layer (Espinosa & Kamm 1999; Halpern *et al.* 1998). For spreading, velocity and pressure scalings are set by a balance between Marangoni stresses and viscous retardation; the important parameters are the viscosity contrast, the initial skin thickness and the Péclet number. For rupture the scalings are set by a balance between pressure and van der Waals forces; here additional parameters arise: dimensionless Hamaker constants and a dimensionless group reflecting the relative importance of Marangoni stresses to van der Waals forces, referred to as the Marangoni parameter. In both cases, numerical simulations of the evolution equations, for a wide variety of parameters, were considered.

The primary conclusions are that the characteristic scalings for spreading can be strongly affected by the addition of the surface layer. In some cases much larger surface deflections are encountered and this may act to block and occlude airways. The surface layer also acts to smooth sharp changes in the solution profiles, and transmits stresses ahead of the surfactant leading edge. The applications to transport in the presence of specific diseases or with specific clinical therapies require an accurate experimental and clinical characterization of both the mucus/PCL depths at various lung generations, and the associated mucus rheology. At present, such precise data are hard to isolate in the literature.

For rupture, one finds that the rupture event can be delayed by the surface film and reverse flows generated by Marangoni stresses, but neither can totally resist the van der Waals forces that drive rupture, provided the layer has thinned sufficiently for them to be active. One finds that increasing the Marangoni effect, thereby apparently promoting stronger reverse flows near the rupture event, leads to earlier rupture; however, the increased Marangoni effects drive a stronger spreading flow thus encouraging rapid thinning and enabling van der Waals forces to become active earlier. Characteristic scalings emerge in the two distinct rupturing situations, either mucus alone rupturing or both PCL and mucus rupturing together; the latter case is much like the rupture of a single layer, and the former follows different scalings verified numerically. Rupture is often an unwanted effect for many coating, painting and adhesive flows, several of which can involve different phases and thus the effects described here will be useful in characterizing when rupture is likely, and how it may be retarded.

M. R. E. W. thanks the EPSRC for funding through a Research Studentship; additional support is through grant GR/N 34895/01. R. V. C. thanks Neil Balmforth (UC Santa Cruz) for many helpful and interesting conversations on a mathematically closely related topic, lava flows, that have undoubtedly had an influence upon this work.

Appendix

Here we provide details of the derivation of the velocity field in the mucus and PCL layers in the modified lubrication approximation. We shall begin by considering the evolution of the upper highly viscous ‘skin-like’ mucus layer.

The leading-order governing equations in the mucus layer become

$$u_{0zz} = 0, \quad -p_{0z} + \eta_1 w_{0zz} = 0, \quad u_{0x} + w_{0z} = 0, \tag{A 1}$$

and to second order we have

$$-p_{0x} + \eta_1[u_{0xx} + u_{2zz}] = 0. \tag{A 2}$$

Similar expansion of the boundary conditions at $z = h_0$ yields

$$u_{0z} = 0, \qquad p_0 - 2\eta_1 w_{0z} = 0, \tag{A 3}$$

to leading order in ϵ and the following to second order:

$$\eta_1[u_{2z} + w_{0x} - 2h_{0x}u_{0x}] + p_0 h_{0x} = \sigma_{0x}. \tag{A 4}$$

From equations (A 1) and (A 3) it can be readily shown that $u_0 \equiv u_0(x,t)$ and the skin velocity is independent of depth; this is a useful simplification that allows considerable progress to be made. This is also the crucial simplification for models of viscous jets and threads, in which the leading-order axial velocity is independent of the radial coordinate. Physically, this is due to the large viscosity of the mucus layer, which makes it resistant to shear to leading order. The function, $u_0(x,t)$ is, however, as yet undetermined. We also note that the pressure is deduced to be $p_0(x,t) = -2\eta_1 u_{0x}$ everywhere within the skin, independent of depth. Using equation (A 2) it can be shown that

$$u_{2z} = 3(h_0 - z)u_{0xx} + F(x,t), \tag{A 5}$$

where $F(x,t)$ is not required for the leading-order dynamics, and integration of the continuity equation in (A 1) yields

$$w_0 = (h_0 - z)u_{0x} + h_{0t} + u_0 h_{0x}. \tag{A 6}$$

Substitution of equations (A 5) and (A 6) into the shear stress in the skin, $\tau_{0xz}(x,z,t) = \eta_1(u_{2z} + w_{0x})$, yields to leading order

$$\tau_{0xz}(x,z,t) = 4\eta_1(h_0 - z)u_{0xx} + 4\eta_1 h_{0x}u_{0x} + \sigma_{0x}. \tag{A 7}$$

Evaluation of τ_{0xz} at the base of the skin, $z = h_0 - \delta_0$, in which δ_0 is the skin thickness, will later be used to fully determine the velocity field.

The leading-order equations in the PCL, $0 < z < h_0 - \delta_0$, are simply given by

$$\bar{u}_{0zz} = \bar{p}_{0x}, \qquad \bar{p}_{0z} = 0, \qquad \bar{u}_{0x} + \bar{w}_{0z} = 0; \tag{A 8}$$

these are the usual governing equations that one obtains in the usual lubrication scaling for the Newtonian-Marangoni-driven single-layer problem (Jensen & Grotberg 1992). At the interface $z = \bar{h}_0$ to leading order, the continuity of velocity, shear stress and normal stress conditions become

$$u_0 - \bar{u}_0 = 0, \quad w_0 - \bar{w}_0 = 0, \quad u_{0z} = 0, \quad 2\eta_1 w_{0z} - p_0 - \bar{p}_0 = 0. \tag{A 9}$$

From (A 8) and (A 9) it can be shown that $\bar{p}_0 = 0$ throughout the PCL liquid layer. To next order

$$\eta_1(u_{2z} + w_{0x} - 2\bar{h}_{0x}u_{0x}) + p_0\bar{h}_{0x} = \bar{u}_{0z}. \tag{A 10}$$

In the PCL layer $\bar{u}_0 \equiv \bar{u}_0(x,z,t)$ and the velocity at the base of the skin is continuous, so $u_0(x,t) = \bar{u}(x, h_0 - \delta_0, t)$. Thus, using the first-order shear stress condition at the interface, (A 10), we obtain

$$\bar{u}_0(x,z,t) = z(\eta_1[u_{2z} + w_{0x} - 2\bar{h}_{0x}u_{0x}] + p_0\bar{h}_{0x})\Big|_{\bar{h}_0} = \left[\frac{u_0}{\bar{h}_0}\right]z.$$

Finally, using continuity of shear stress at $z = \bar{h}_0$ we obtain an evolution equation for $u_0(x,t)$ as

$$u_0(x,t) = \bar{h}_0[4\eta_1\delta_0 u_{0xx} + 4\eta_1(h_{0x} - \bar{h}_{0x})u_{0x} + \sigma_{0x}]. \quad \text{(A 11)}$$

This equation must be solved to determine $u_0(x,t)$, and hence the velocity everywhere in the liquid layer.

The evolution equations for $\bar{h}_0$, h_0 and Γ_0 are determined using the leading-order kinematic boundary conditions at $z = h_0$ and $z = \bar{h}_0$ and the equation of surfactant mass conservation at $z = h_0$.

REFERENCES

Balmforth, N. J. & Craster, R. V. 2000 Dynamics of cooling domes of viscoplastic fluid. *J. Fluid Mech.* **422**, 225–247.

Balmforth, N. J. & Craster, R. V. 2002 A skin theory for cooling lava domes. In preparation.

Banerjee, R. & Puniyani, R. R. 2000 Exogenous surfactant therapy and mucus rheology in chronic obstructive airway diseases. *J. Biomater. Appl.* **14**, 243–272.

Blom, J. G. & Zegeling, P. A. 1994 Algorithm 731: a moving-grid interface for systems of one-dimensional time-dependent partial differential equations. *ACM Trans. Math. Software* **20**, 194–214.

Borgas, M. S. & Grotberg, J. B. 1988 Monolayer flow on a thin film. *J. Fluid Mech.* **193**, 151–170.

Bull, J. L., Nelson, L. K., Walsh, J. T., Gluckberg, M. R., Schurch, S. & Grotberg, J. B. 1999 Surfactant spreading and surface-compression disturbance on a thin viscous films. *J. Biomech Engng* **121**, 89–98.

Burelbach, J. P., Bankoff, S. G. & Davis, S. H. 1988 Nonlinear stability of evaporating condensing liquid-films. *J. Fluid Mech.* **195**, 463–494.

Craster, R. V. & Matar, O. K. 2000 Surfactant transport on mucus films. *J. Fluid Mech.* **425**, 235–258 (referred to herein as Paper I).

Craster, R. V., Matar, O. K. & Papageorgiou, D. T. 2002 Pinchoff and satellite formation in surfactant covered viscous threads. *Phys. Fluids* **14**, 1364–1376.

De Wit, A., Gallez, D. & Christov, C. I. 1994 Nonlinear evolution equations for thin liquid films with insoluble surfactants. *Phys. Fluids* **6**, 3256–3266.

Edwards, D. A., Brenner, H. & Wasan, D. T. 1991 *Interfacial Transport Processes and Theology*. Butterworth-Heinemann.

Erneux, B. T. & Davis, S. H. 1993 Nonlinear rupture of free films. *Phys. Fluids* A **5**, 1117–1122.

Espinosa, F. F. & Kamm, R. D. 1999 Bolus dispersal through the lungs in surfactant replacement therapy. *J. Appl. Physiol.* **86**, 391–410.

Espinosa, F. F., Shapiro, A. H., Fredberg, J. J. & Kamm, R. D. 1993 Spreading of exogenous surfactant in an airway, *J. Appl. Physiol.* **75**, 2028–2039.

Gaver III, D. P. & Grotberg, J. B. 1990 The dynamics of a localized surfactant on a thin film. *J. Fluid Mech.* **213**, 127–148.

Grotberg, J. B. 1994 Pulmonary flow and transport phenomena, *Annu. Rev. Fluid Mech.* **26**, 529–571.

Grotberg, J. B., Halpern, D. & Jensen, O. E. 1995 Interaction of exogenous and endogenous surfactant: spreading rate effects. *J. Appl. Physiol.* **78**, 750–756.

Halpern, D. & Grotberg, J. B. 1992 Dynamics and transport of a localized soluble surfactant on a thin film. *J. Fluid Mech.* **237**, 1–11.

Halpern, D., Jensen, O. E. & Grotberg, J. B. 1998 A theoretical study of the surfactant and liquid delivery into the lung. *J. Appl. Physiol.* **85**, 333–352.

Harlen, O. G., Rallison, J. M. & Chilcott, M. D. 1990 High-Deborah-number flows of dilute polymer solutions, *J. Non-Newtonian Fluid Mech.* **34**, 319–349.

Ida, M. P. & Miksis, M. J. 1998*a* The dynamics of thin films I: General theory. *SIAM J. Appl. Maths* **58**, 456–473.

Ida, M. P. & Miksis, M. J. 1998*b* The dynamics of thin films II: Applications. *SIAM J. Appl. Maths* **58**, 474–500.

Israelachvili, J. N. 1985 *Intermolecular and Surface Forces With Applications to Colloidal and Biological Systems*. Academic.

Jensen, O. E. 1994 Self-similar, surfactant driven flows. *Phys. Fluids* **6**, 1084–1094.

Jensen, O. E. & Grotberg, J. B. 1992 Insoluble surfactant spreading on a thin viscous film: shock evolution and film rupture. *J. Fluid Mech.* **240**, 259–288.

Jensen, O. E. & Grotberg, J. B. 1993 The spreading of heat or soluble surfactant along a thin film. *Phys. Fluids* A **5**, 58–68.

Jensen, O. E. & Halpern, D. 1998 The stress singularity in surfactant-driven-film flows. Part 1. Viscous effects. *J. Fluid Mech.* **372**, 273–300.

Keast, P. & Muir, P. H. 1991 Algorithm 688 EPDCOL – a more efficient PDECOL Code. *ACM Trans. Math. Software* **17**, 153–166.

Matar, O. K. & Troian, S. M. 1998 Growth of non-modal transient structures during the spreading of surfactant coated films. *Phys. Fluids* **10**, 1234–1237.

Matar, O. K. & Troian, S. M. 1999*a* The development of transient fingering patterns during the spreading of surfactant coated films. *Phys. Fluids* **11**, 3232–3246.

Matar, O. K. & Troian, S. M. 1999*b* Spreading of a surfactant monolayer on a thin liquid film: Onset and evolution of digitated structures. *Chaos* **9**, 141–153.

Naire, S., Braun, R. J. & Snow, S. A. 2000 Limiting cases of gravitational drainage of a vertical free film for evaluating surfactants. *SIAM J. Appl. Maths* **61**, 889–913.

Papageorgiou, D. T. 1995*a* Analytical description of the breakup of liquid jets. *J. Fluid Mech.* **301**, 109–132.

Papageorgiou, D. T. 1995*b* On the breakup of viscous liquid threads. *Phys. Fluids* **7**, 1529–1544.

Robertson, B. 1984 *Pulmonary Surfactant*. Elsevier.

Ruckenstein, E. & Jain, R. K. 1974 Spontaneous rupture of thin liquid films. *Chem. Soc. Faraday Trans.* **70**, 132–137.

Saffman, P. G. 1976 Brownian motion in thin sheets of viscous fluid. *J. Fluid Mech.* **73**, 593–602.

Scriven, L. E. 1960 Dynamics of a fluid interface: Equation of motion for Newtonian surface fluids. *Chem. Engng Sci.* **12**, 98–108.

Sharma, A. & Ruckenstein, E. 1986 An analytical nonlinear theory of thin film rupture and its applications to wetting films. *J. Colloid Interface Sci.* **113**, 456–479.

Silberberg, A. 1983 Biorheological matching, mucociliary interaction and epithelial clearance. *Biorheology* **20**, 215–222.

Sincovec, R. F. & Madsen, N. K. 1979 Algorithm 540 PDECOL. *ACM Trans. Math. Software* **5**, 326–351.

Sleigh, M. A. 1991 Mucus Propulsion. In *The Lung: Scientific Foundations* (ed. R. G. Crystal and J. B. West), chap. 3.1.4. Raven Ltd, New York.

de Souza, E. R. & Gallez, D. 1998 Pattern formation in thin liquid films with insoluble surfactants. *Phys. Fluids* **10**, 1804–1814.

Stone, H. A. 1990 A simple derivation of the time-dependent convective-diffusion equation for surfactant transport along a deforming interface. *Phys. Fluids* A **2**, 111–112.

Stone, H. A. 2000 Philip Saffman and viscous flow theory. *J. Fluid Mech.* **409**, 165–183.

Toniolo, C. 2001 Slipping instability in a system of two superposed fluid layers. In *Proc. 2001 GFD Summer School*. Woods Hole Oceanographic Institution.

Warner, M. R. E., Craster, R. V. & Matar, O. K. 2002 Unstable van der Waals driven line rupture in Marangoni driven thin viscous films. *Phys. Fluids* **14**, 1642–1654.

Williams, M. B. & Davis, S. H. 1982 Nonlinear theory of film rupture *J. Colloid Interface Sci.* **90**, 220–228.

Witelski, T. P. & Bernoff, A. J. 1999 Stability of self-similar solutions for van der Waals driven thin film rupture. *Phys. Fluids* **11**, 2443–2445.

Witelski, T. P. & Bernoff, A. J. 2000 Dynamics of three-dimensional thin film rupture. *Physica* D **147**, 155–176.

Zhang, W. W. & Lister, J. R. 1999*a* Similarity solutions for capillary pinch-off in fluids of differing viscosity. *Phys. Rev. Lett.* **83**, 1151–1154.

Zhang, W. W. & Lister, J. R. 1999*b* Similarity solutions for van der Waals rupture of a thin film on a solid substrate. *Phys. Fluids* **11**, 2454–2462.